JCTC Journal of Chemical Theory and Computation

Article

pubs.acs.org/JCTC

More π Electrons Make a Difference: Emergence of Many Radicals on Graphene Nanoribbons Studied by *Ab Initio* DMRG Theory

Wataru Mizukami, Yuki Kurashige, and Takeshi Yanai*

Department of Theoretical and Computational Molecular Science, Institute for Molecular Science, Okazaki, Aichi 444-8585, Japan

Supporting Information

ABSTRACT: Graphene nanoribbons (GNRs), also seen as rectangular polycyclic aromatic hydrocarbons, have been intensively studied to explore their potential applicability as superior organic semiconductors with high mobility. The difficulty arises in the synthesis or isolation of GNRs with increased conjugate length, GNRs being known to have radical electrons on their zigzag edges. Here, we use a most advanced *ab initio* theory based on density matrix renormalization group (DMRG) theory to show the emerging process of how GNRs develop electronic states from nonradical to radical characters with increasing ribbon length. We show the mesoscopic size effect that comes into play in quantum many-body interactions of π electrons, which is responsible for the polyradical nature. An analytic form is presented to model the size dependence of the number of radicals for arbitrary-length GNRs. These results and associated insights deepen the understanding of carbon-based chemistry and offer useful information for the synthesis and design of stable and functional GNRs.

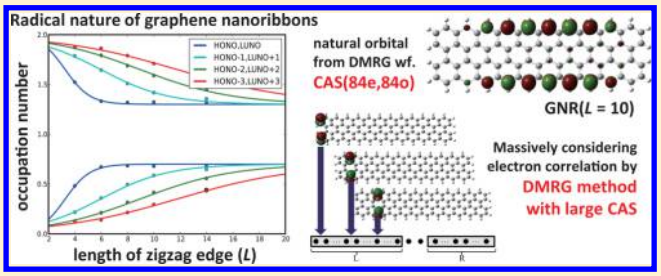

1. INTRODUCTION

In complex or conjugated systems, remarkable properties that are not simply deducible from the nature of the basic building blocks may develop beyond our imagination. Graphene nanoribbons (GNRs) exhibit such intriguing electronic phenomena, which emerge as unexpected outcomes of collective motion of conjugated π electrons. The entanglements of π electrons are closed in a low-dimensional honeycomb topology incorporated into confinement with edge boundaries. As such an emergent feature, this study describes the building of multiple radicals in semi-infinite GNRs of the ground (singlet) state as well as its quantitative characterization by using a sophisticated computational method.

As illustrated in Figure 1, finite-size GNRs have two kinds of edges: *zigzag* and *armchair* edges. In this article, unless otherwise mentioned, we refer to GNRs as rectangular GNRs in a zigzag configuration. In this shape, the sizes of the armchair and zigzag edges, which correspond to the *width* and *length* of a ribbon, respectively, are denoted by W and L, respectively (see Figure 1). A varied size of a GNR is labeled as GNR[W,L].

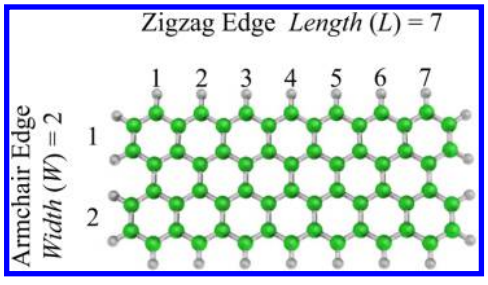

Figure 1. Zigzag-edge graphene nanoribbons (GNR) with W (width) = 2 and L (length) = 7 (i.e., GNR[2,7]).

GNRs are candidates for future organic semiconductors, since they are thought to have significant potential for high conductivity.[1−3] At present, an example of a practical semiconducting molecular material of the GNR type is only pentacene, equivalently written as GNR[1,5]. Although pentacene's charge-carrier mobility is high as compared with those of other organic materials, there yet remain strong demands for superior GNR-based materials that possess much higher carrier mobility for low-voltage organic transistors. Infinite (or bulk) graphene sheets have zero band gap character[4] and thus cannot be straightforwardly applied to electronic devices such as transistors, though they hold the record of room-temperature thermal conductivity.[5] The finitely terminated width (or length) of GNRs is responsible for the finite energy gaps between the ground and excited states, ensuring a potential applicability to semiconductors. The electric properties and energy gaps of GNRs are expected to be highly tunable by controlling their ribbon widths.[6] An increase in L (and W) of GNRs is a possible direction to enhancing mobility in a way that the conductivity bears an asymptotic resemblance to those of bulk graphene.

Despite increasing interest in GNRs, the synthesis of long-chain GNRs poses an enormous challenge, while some marked progress has recently been shown, e.g., synthesis of nonacene, teranthene, etc.[7,8] The difficulty lies in the chemical and thermal instability of the long GNRs, which are seemingly

Received: October 15, 2012
Published: November 20, 2012

dx.doi.org/10.1021/ct3008974 | J. Chem. Theory Comput. 2013, 9, 401−407

prone to a radical nature. It leads to high reactivity that hinders the synthesis of isolated systems. In conjunction with experimental efforts, numerous theoretical investigations[9−30] to expand analytic insight into the electronic properties and stability have been pursued, particularly for polyacenes, or GNR[1,L]. As a result of recent studies, the ground state of longer-chain polyacenes is characterized as the open-shell singlet,[31−36] which can alternatively be viewed as the emergence of radical electrons or polyradicals.[33] In general, the radical nature is considered to be intrinsic to GNRs (polyacenes and beyond).[9,10]

It has been theoretically and experimentally shown that GNRs have nonbonding π electrons that are coherently localized on both zigzag edges.[9,10,37] The radical electrons arise on top of these localized π orbital states, known as edge states. The presence of the edge states is important to valuing GNRs as materials for semiconductors as well as spintronics devices.[18,20−24,29,30] The earlier theoretical studies on the GNRs ($W > 1$) exclusively relied on mean-field approaches, such as the tight-binding model and density functional theory (DFT). They described the radicals in the sense that two opposite spins are each localized on a different side of the zigzag edges, forming an antiferromagnetic state. This radical picture was simulated by the spin-polarized treatment, which mimics electron correlation as a limit of the classical spin model. It can be conversely indicated that the relationship between radicals and edge states in GNRs is built upon the role of electron correlation.

An infinite limit of the radical character with increasing GNR length was surmised by the previous band structure calculations, resulting in a macroscopic description of an infinite number of radicals on the zigzag edges. At the other extreme, the short GNRs, such as benzene, anthracene, perylene, etc., are closed-shell (nonradical) molecules. Such a remarkable difference between these two extremes can be regarded as an example of the "more is different" phenomenon. This study describes the emerging feature of GNRs, the electronic states of which evolve from nonradical to many-radical states with an increase in the ribbon length. The questions are, what size of GNR shows *di*-radical, *tetra*-radical, or higher-order radical characters? How many "more" π electrons give rise to what difference? We attempt to constitute a "missing link" in our understanding of the radical nature of GNRs ranging from short to semi-infinite scales by considering as much electron correlation associated with quantum fluctuation as possible, where the cutting-edge *ab initio* quantum chemistry approach is reachable.

2. METHODS

2.1. Quantum-Chemical Density Matrix Renormalized Group (DMRG) Calculations. Radical structures are manifested in conjugated π electrons in an open-shell configuration. These open-shell singlet radicals are conceived of as-correlated (or resonating) π electronic states which can be formulated as the superposition of several electronic configurations. In our calculations, the radical states of GNR[W,L]'s were accounted for by considering a full set of the configurations arising from $W \times (4L + 2)$ valence π electrons, which are energetically competitive. Our *ab initio* computational approach faced a great complexity of having a huge number of configurations interact in a nonperturbative fashion, capturing the nature of the so-called *multireference* electronic states. The density matrix renormalization group (DMRG) theory,[38,39] adapted to quantum chemistry calculations for multireference electronic systems,[40−43] enabled us to determine the radical or nonradical singlet states with the full valence π (see section 2.2). Acenes were previously studied by Hachmann et al. similarly using the DMRG wave function with the π active space, suggesting their polyradical nature.[33] Meanwhile, the present study has dealt with greater complexity to extend the scope to the GNRs with $W = 2$.

As shown in Supporting Information section 1, the DMRG calculations predicted that GNRs (as well as acenes[33]) possess the singlet ground state for all the lengths considered. The longer GNRs were then found to have an increasingly rising amount of electron correlation, which the single reference of the spin-polarized DFT failed to catch up with (see Figure S2). Supporting Information section 2 addresses the accuracy concerns in the DMRG calculations, which is known to be the most efficient approach for one-dimensional systems, whereas GNR's width may create another dimensionality, which is not in general favorable for the approximation to correlation network in DMRG.

2.2. Computational Details. Multireference electronic structure calculations on GNRs were performed using an *ab initio* DMRG method, which was implemented into an efficient parallel computer program by our group. The DMRG method was incorporated into the active space model, in which a finite set of molecular orbitals, obtained by the preceding restricted Hartree−Fock quantum chemistry calculations with Gaussian-type atomic orbital basis functions (6-31G basis sets), was divided into active and external sets. The DMRG was used to describe electron correlation within the active space, circumventing the prohibitive cost of full configuration interaction in the complete π active space. A full set of the valence π orbitals and associated π electrons of the systems were selected as the active space, resulting in an effective correlated π-conjugated system of $W \times (4L + 2)$ electrons with $W \times (4L + 2)$ orbitals for GNR[W,L] (e.g., 132 electrons with 132 orbitals for GNR[2,16]). Molecular orbitals in active space were localized using the Pipek−Mezey population-localization method[44] under C_{2v} symmetry constraints so as to transform the orbitals into efficient local sites for the DMRG calculations of the 1D ribbon systems (see Figure 2). Related to this, the ordering of the localized active orbitals was specified to assign them to the 1D lattice sites of DMRG algorithm.

Ab initio DMRG is formulated by mapping molecular orbitals to one-dimensional lattice sites. The DMRG wave function is optimized in this 1D space. It is well-known from earlier DMRG studies that orbital ordering significantly affects the convergence of correlation energies with respect to the number of renormalized basis states (M). The computational cost of DMRG is formally $O(M^2N^4 + M^3N^3)$, where N denotes the number of active orbitals. The efficiency of *ab initio* DMRG calculation depends on the ordering of active orbitals on the 1D lattice. An approach recently proposed to determine optimal orbital ordering is the minimization of the bandwidth of the matrix whose element represents an interaction between active orbitals. Chan et al. showed a way to find orbital ordering by minimizing the bandwidth of the one-electron bare core Hamiltonian integral matrix with the symmetric reverse Cuthill−McKee (RCM) reordering algorithm.[46] We determined the orbital ordering using the minimization of the bandwidth of the exchange integral matrix K_{ij}, where i and j indicate the localized molecular orbitals. The matrix elements of exchange matrix K_{ij} directly reflect the distances and overlaps

dx.doi.org/10.1021/ct3008974 | J. Chem. Theory Comput. 2013, 9, 401−407

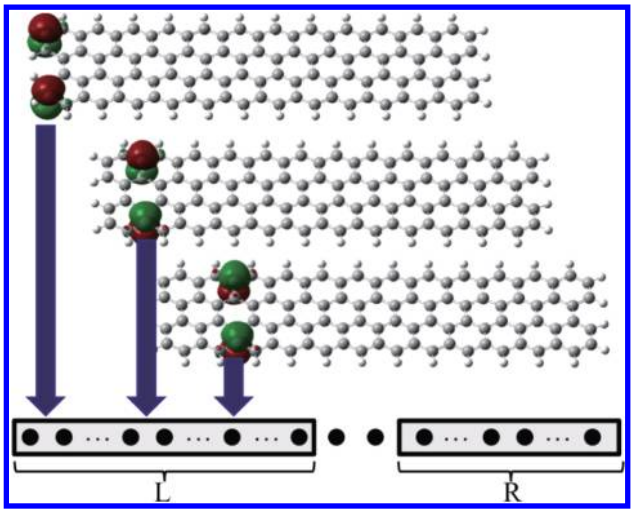

Figure 2. Schematic illustration of the orbital ordering of localized orbitals assigned to the 1D lattice sites of DMRG. Schematic illustration of the orbital ordering of localized orbitals assigned to the 1D lattice sites of DMRG. Molecular orbitals were localized subject to the constraint of C_{2v} symmetry, as illustrated (green and red surfaces). The localized orbitals were mapped to the one-dimensional lattice space for the DMRG sweeping algorithm. A sweeping configuration is schematized at the bottom of the figure. This mapping, namely the ordering of localized orbitals in the 1D space, was determined by minimizing the bandwidth of the exchange matrix $K_{ij} = (ijlij)$.

between localized orbitals. As another aspect, K_{ij} may be nonzero even if *i,j* orbitals belong to different symmetries. The exchange matrix was already adopted by Moritz et al. as an optimal interaction matrix in conjunction with the RCM reordering method,[47] though it is not always the best choice. In this study, to minimize the bandwidth, we employed the Minimum Bandwidth by Perimeter Search (MB-PS) method.[48] While RCM is a heuristic approach to reduce the bandwidth of the matrix (in particular large sparse matrix), the MB-PS method is the technique to find an exact solution for bandwidth minimization problems. This scheme used maybe a more robust approach to the orbital ordering problems.

The one-electron reduced density matrix was computed from the DMRG wave function during the two-sites sweeping procedure and was then diagonalized to obtain natural orbitals and the corresponding occupation numbers (NOONs) as eigenvectors and eigenvalues, respectively. The NOONs shown in Figure 3 were evaluated from the DMRG calculations that used 1024 renormalized basis states to represent the wave function in the DMRG algorithm. Figures 4 and 5 are based on the DMRG results achieved with 256 and 512 renormalized basis states for $W = 1$ and 2, respectively. In the present DMRG calculations, orbital relaxation arising in the correlated active orbitals was not taken into account. Note that our DMRG wave function was spin-adapted. Supporting Information section 1 shows the singlet−triplet energy gaps, which were evaluated as a relative energy difference between the separate DMRG calculations for singlet and triplet states.

In this study, two sets of molecular structures of GNRs were employed. Figure 3 gives the results of the geometries optimized with density-functional theory (DFT) calculations with D_{2h} point group symmetry, while the calculations for Figures 4 and 5 were performed using the model geometries. The spin-polarized DFT calculations for the geometry optimization were performed using the Gaussian 09 program package[49] at the CAM-B3LYP/6-31G* level of theory. Geometric parameters of the model GNR structures are 1.010 Å for the carbon−hydrogen (C−H) bond length, 1.402 Å and 1.435 Å for the carbon−carbon (C−C) bond length along the zigzag and armchair directions, respectively, and 120.0° for the C−C−C bond angle. It should be mentioned that the radical character was not sensitive to the geometric parameters in our calculaitons (see Supporting Information section 3).

Using a minimal basis (STO-3G) for computational convenience, MP2 and orbital-optimized MP2 calculations were performed using the ORCA program package[50] with the resolution-of-identity approximation for Coulomb operators, in which Ahlrichs's valence double-ζ set[51] was used as auxiliary basis functions. MP2 natural orbitals and associated occupation

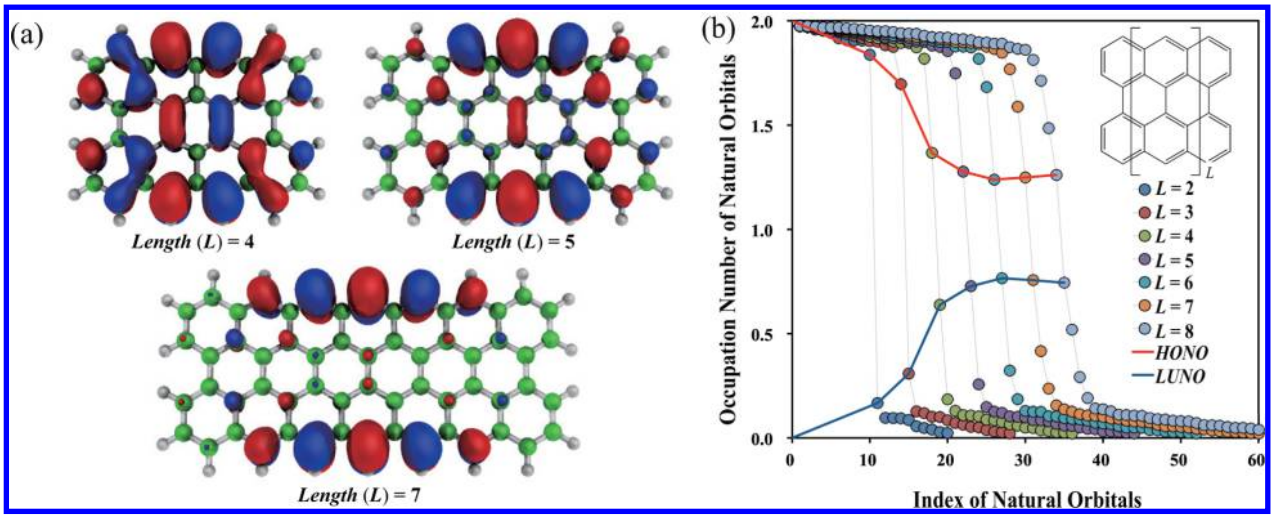

Figure 3. Emergence of radical characters in GNRs with $W = 2$. (a) Plots (red and blue surfaces) of the Highest Occupied Natural Orbitals (HONOs) of GNRs with $W = 2$ and $L = 4$, 5, and 7. Progressive localization on the zigzag edges is caused with increasing L. (b) Natural Orbital Occupation Numbers (NOONs) of π orbitals of GNR chains with $W = 2$ and $L = 2$−8 in the singlet state. Two trends (guided by lines) show the occupancies of HONOs (upper) and LUNOs (lower), respectively, which are closer to 1 (singly occupied) than the other orbitals.

dx.doi.org/10.1021/ct3008974 | J. Chem. Theory Comput. 2013, 9, 401−407

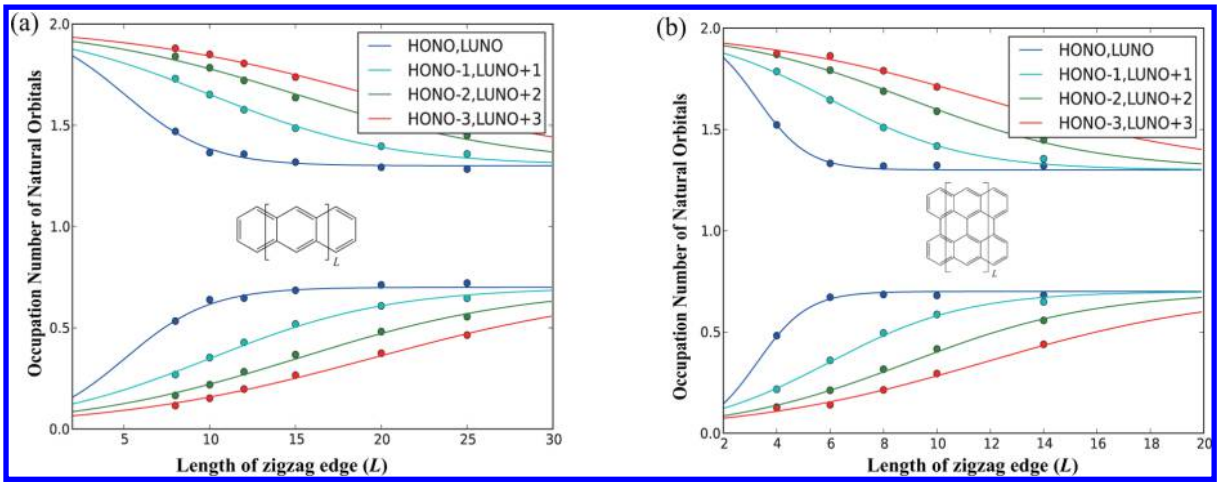

Figure 4. Hyperbolic-tangent model of length dependence of natural orbital occupation numbers (NOONs) for (a) acenes (GNR[1,L]) and (b) GNR[2,L]. Circles are the calculated NOONs of HONO − i/LUNO + i (i = 0−4). The modeled functions (lines) are given by eqs 1 and 2, which are parametrized with the hyperbolic tangent function. The extrapolation of occupancies using these analytic expressions provides a connection of multiple emerging states, ranging from closed-shell to open-shell characters.

numbers for evaluation of the radical index R (Figure 5) were provided by ORCA. The validity of MP2/STO-3G is discussed in Supporting Information section 3 as well as that of model geometries.

3. RESULTS AND DISCUSSION

We present the description of the calculated electronic structures of GNRs in the singlet state. Natural orbitals and associated occupation numbers (NOONs) were computed from the correlated DMRG wave function (Figure 3). The NOON represents the number of electrons on a natural orbital and ranges from 0 (unoccupied) to 2 (doubly occupied). In the present theory, the open shell or radical is modeled as a noninteger deviation in the occupancy from 0 or 2, approaching 1 (singly occupied). Two orbitals with the NOONs closest to 1 are designated as the "highest occupied natural orbital" (HONO) with occupancy greater than 1 and the "lowest unoccupied natural orbital" (LUNO) with occupancy less than 1. In the single reference limit for closed-shell systems, the HONO and LUNO converge to the highest occupied molecular orbital (HOMO) and lowest unoccupied molecular orbital (LUMO), respectively.

Figure 3a shows the HONOs of GNRs with W = 2 and L = 4, 5, and 7. HONOs and LUNOs of longer GNRs are progressively localized on the zigzag edges. Such localization of the valence π orbitals, also known as the *edge effect*, was already observed in earlier theoretical studies based on mean-field models, such as the tight-binding model and DFT. It is thus indicated that the edge orbital states arise regardless of the presence of the high-level electron correlation and consequently are ascribed to the topological interaction in a honeycomb lattice as well as the finite termination that leads to the so-called quantum confinement.

Figure 3b is a plot of NOONs of active π space for GNR chains with W = 2 and L = 2−8 in the singlet state. The occupancy of HONO is 1.84, 1.37, and 1.25 for L = 2, 4, and 7, respectively, and that of LUNO is 0.17, 0.64, and 0.76 for L = 2, 4, and 7, respectively. Thus, the characters of HONO and LUNO both approach single-electron occupation for longer GNRs. This size dependence of the occupancies is a description of the emerging of *di*-radical character in GNRs.

This singlet state having the near single occupations (i.e., open-shell singlet) means that its description formally requires the use of the multireference (or multideterminantal) wave function. Alternatively, the electron correlation to account for quantum fluctuation of spins is highly responsible, as mentioned earlier. Coulomb repulsion with such high-level correlation increases the effective mass of electrons, so that the heavy electrons are each apt to localize on a single site, leading to localized, unpaired π electrons, which are viewed as radicals. From this perspective, electron correlation seems to enhance the edge effect.

In addition, the populations of unpaired electrons in the second HONO and LUNO, denoted by HONO−1 and LUNO +1, respectively, rise as GNRs increase in length. The HONO−1 (LUNO+1) has an occupancy of 1.91 (0.10), 1.82 (0.19), and 1.59 (0.42) electrons for GNR[2,L] with L = 2, 4, and 7, respectively. As seen in Figure 3b, the continuous growing of multiple open-shell electrons in HONO−i and LUNO+i for i = 0, 1, 2... reveals that longer GNRs build increasingly more radicals.

We have described finite-length GNRs (L = 2−8) using a molecular approach, but can we stretch this finite-length description into an arbitrary length toward infinity? In what follows, we present our approach to bridge a gap in the radical picture between short- and infinite-length GNRs. We here introduce a model to generalize the length-dependence of the occupancy in an algebraic fashion. This generalization was deduced from the calculated NOONs along with the following fitting functions:

$$f(L)^{\mathrm{HONO}-i} = 2 - h\{1 + \tanh(a_i(L - b_i))\} \quad (1)$$

$$f(L)^{\mathrm{LUNO}+i} = 2 - f(L)^{\mathrm{HONO}-i} \quad (2)$$

which give the occupancies of HONO−i and LUNO+i, respectively, for a given length L. The values of the parameters a_i, b_i, and h were determined from the NOONs that were obtained by performing the DMRG calculations on GNR[2,L] with L up to 14 as well as acenes (GNR[1,L]) with L up to 25 where the computationally intensive calculations were permitted. The resultant values are shown in Supporting Information section 4. We found that h is constant (h = 0.35).

dx.doi.org/10.1021/ct3008974 | J. Chem. Theory Comput. 2013, 9, 401−407

Figure 4 displays the fitted functions of eqs 1 and 2 for $i = 0-3$ along with the computed NOONs. A comparison can be made between acenes (Figure 4a) and GNRs with $W = 2$ (Figure 4b).

Using these modeled occupation numbers, we readily estimate the radical character of GNRs with any length up to semi-infinity. Let us define a single radical electron as the occupancy in the range of 0.5−1.5. This definition simply allows us to count how many radicals emerge for a given-length GNR. We then found that GNR[2,L] is closed-shell for $L < 4$, *di*-radical for $4 \leq L < 8$, *tetra*-radical for $8 \leq L < 12$, *hexa*-radical for $12 \leq L < 16$, and *octa*-radical or higher-order for $L \geq 16$ (Figure 4b). In acenes (GNR[1,L]), the radical character is shown to be nonradical for $L < 7$, *di*-radical for $7 \leq L < 15$, *tetra*-radical for $15 \leq L < 21$, *hexa*-radical for $21 \leq L < 27$, and *octa*-radical or higher-order for $L \geq 27$ (Figure 4a). Going beyond *octa*-radical character, GNRs keep creating radical electrons proportional to L; two radical electrons arise from an increase in length of three for GNR[2,L] and of five for acenes. This clearly suggests a width effect that accelerates the length-dependence of radicals for wider GNRs: GNR[2,L] has a higher rate of building radicals than acenes (GNR[1,L]) with an increase in the length.

Here is shown our insight into further modeling of occupation numbers. The parameter a_i can be expressed as the following exponential function: $a_i = p \exp(-q(i - r)) + s$, where p, q, r, and s are the fitting parameters for GNR[W,L] with a given W. The optimized values of p, q, r, and s for $W = 1$ and 2 are shown in Table S4. If we were to further establish the width-dependence of these parameters, the occupancies of any-size GNRs would be modeled. This requires the calculations to be extended to wider GNRs, which are, however, out of reach with the present approach.

An alternative characterization of GNR's radicals can be performed using Head-Gordon's radical index,[33,52] which is given by $R = \sum_i^N \min(n_i, 2 - n_i)$, where n_i refers to the ith NOON of N valence π orbitals. This measure accounts for the effective number of unpaired electrons and provides a simple and unified insight into differences in radical characters among various-length GNRs. Figure 5 plots the values of R obtained from DMRG calculations for acenes ($W = 1$) and GNRs ($W = 2$) along with those calculated at the second-order Møller−Plesset perturbation (MP2) level of theory. The MP2 method describes the lowest-order perturbative correlation, and thus a comparison of the radical index between the MP2 and DMRG results highlights the effect of higher-order nonperturbative correlation. The trends of R shown in Figure 5 all exhibit a linear dependence on L. This means that n-radical characters (n = *di*, *tetra*, *hexa*, ...) consecutively develop as the length of GNRs increases. A comparison of R between $W = 1$ and 2 indicates that a greater width (W) creates a stronger L-dependence of the number of radical electrons. As also observed in DMRG calculations, the NOON of HONO from MP2 calculations approaches 1 by increasing the length; for example, the HONO (LUNO) with $W = 2$ is occupied by 1.83 (0.17) and 1.53 (0.47) electrons for $L = 4$ and 8, respectively.

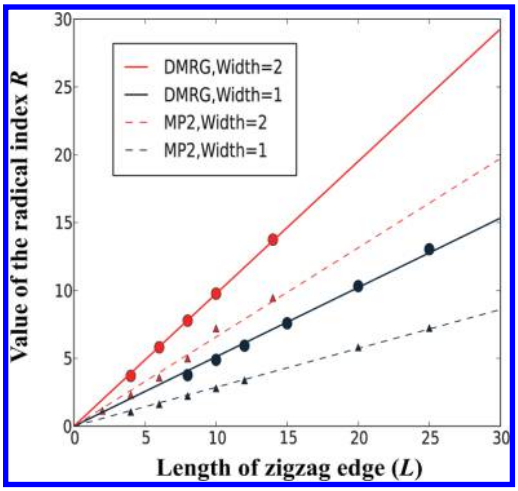

Figure 5. Radical index R of GNR[W,L] with $W = 1$ and 2. Radical index R is a measure of the number of radicals and defined in the main text. Dashed lines along with triangles represent R evaluated by the MP2 method that considers only weak electron correlation. Solid lines along with circles indicate R using the DMRG method that is designed to describe strong (higher-order) correlation.

It was clearly illustrated that the higher-order correlation accelerates the rising of radical electrons, and this ensures the strong relation between electron correlation and radicals. In the DMRG prediction, for example, *di*-radical and *tetra*-radical characters arise in GNR[2,L] with $L = 4$ and 8, respectively, which gives the radical index $R = 3.7$ and 7.8, respectively. These values of the radical index were produced in the MP2 model with GNR[2,L] with $L = 6$ and 12, respectively, and this means that the MP2 method underestimates the number of radicals. Note that the MP2 wave function was at first glance qualitatively able to capture the rising radicals of GNRs,[53] while it gave an unphysical description for the energetics (see Supporting Information section 5).

We investigated the feature of electron correlation in GNRs using spin−spin correlation functions. Two types of spin−spin correlation functions were evaluated: One is defined as $C_{ij} = \langle \hat{S}_i^z \hat{S}_j^z \rangle$; the other is $\tilde{C}_{ij} = \langle \hat{S}_i^z \hat{S}_j^z \rangle - \langle \hat{S}_i^z \rangle - \langle \hat{S}_j^z \rangle$. The latter $\tilde{C}_{ij}$ measures the difference from the one-body contribution, highlighting the correlation associated with quantum spin fluctuation. Here, i and j are the indices of the symmetry-constrained localized molecular orbitals (LMOs) used as the 1D lattice sites of DMRG calculations (see Figure 2). The computed spin−spin correlation functions C_{ij} and $\tilde{C}_{ij}$ were presented in Figure 6. This has uncovered a surprising correlation nature of GNRs. The matrix plots of the correlation functions were shown to be diagonally dominant and can be seen as a sparse band matrix. This presumably means that the electronic structure of GNRs is governed by short-range multireference correlation between local spins.[33] This is in contrast to long-range correlation observed in our previous study on multisite carbene organic molecules, whose singlet state is likewise polyradical and antiferromagnetic.[54] The short-range nature of correlation found in GNRs can perhaps explain why MP2 gave the qualitatively correct behavior of the radical index as a linear function of L.

4. CONCLUSION

In summary, this work illustrated an emergening phenomenon in chemistry. We quantitatively described the building process of radicals in GNRs which develop from nonradical to polyradical characters with increasing ribbon length. Our method which considered a large amount of nonperturbative electronic interaction revealed the mesoscopic size effect where complex correlations of many electrons strongly promote the emergence of radical electrons on edge orbital states. The electric ground state of GNRs evolves from nonradical single-reference character to polyradical character smoothly when

dx.doi.org/10.1021/ct3008974 | J. Chem. Theory Comput. 2013, 9, 401−407

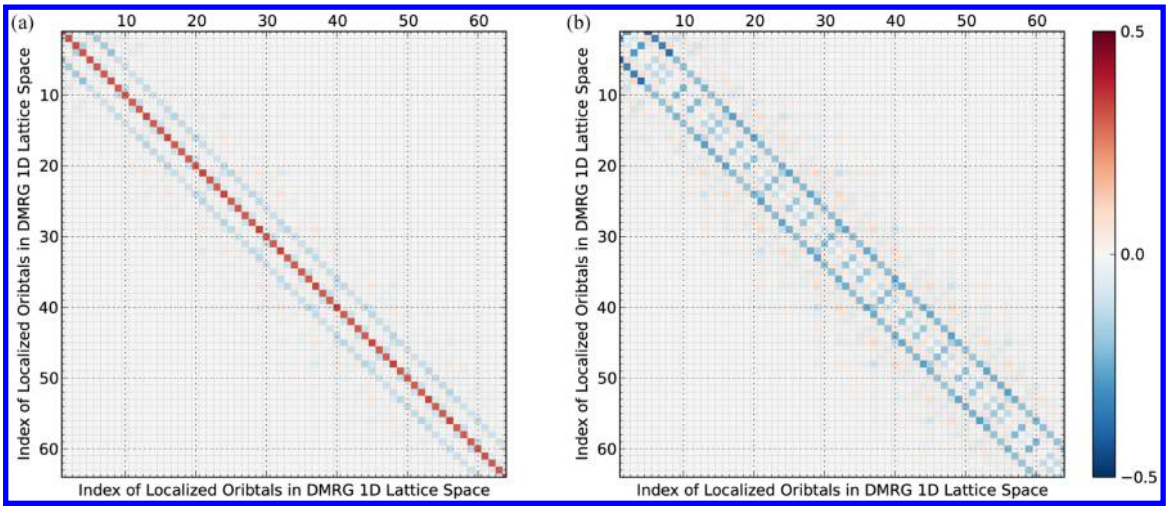

Figure 6. Correlations between localized molecular orbitals (LMO) of GNRs in terms of spin−spin correlation functions C_{ij} (left) and $\tilde{C}_{ij}$ (right). Each i and j indicates a localized molecular orbital (LMO) in the 1D lattice sites of DMRG (a) spin−spin correlation including meanfiled effects: $C_{ij} = \langle \hat{S}_i^z \hat{S}_j^z \rangle$ (b) spin−spin correlation without meanfiled contributions: $\tilde{C}_{ij} = \langle \hat{S}_i^z \hat{S}_j^z \rangle - \langle \hat{S}_i^z \rangle - \langle \hat{S}_j^z \rangle$.

incorporating more π electrons. Furthermore, the advent of higher-order radical characters was modeled in an analytic form. This model enables us to know how many radical electrons are present on GNR's edges, serving as a certain bridge between molecular and bulk GNRs. Such information should be valuable in the synthesis of stable GNRs and the design of functional organic materials with potential conductivity.

■ ASSOCIATED CONTENT

Supporting Information

Further calculation details such as singlet−triplet gaps discussed in the text. This material is available free of charge via the Internet at http://pubs.acs.org/.

■ AUTHOR INFORMATION

Corresponding Author

*E-mail: yanait@ims.ac.jp.

Notes

The authors declare no competing financial interest.

■ ACKNOWLEDGMENTS

This research was supported in part by the Core Research for Evolutional Science and Technology Program, High Performance Computing for Multi-Scale and Multi-Physics Phenomena of the Japan Science and Technology Agency (JST), and Young Scientists (B) (Grant No. 21750028) and Grant-in-Aid for Scientific Research (C) (Grant No. 21550027) from Ministry of Education, Culture, Sports, Science and Technology—Japan (MEXT). W.M. thanks the Canon Foundation for financial support. W.M. is indebted to Prof. Kenji Yonemitsu for helpful comments and fruitful discussions.

■ REFERENCES

(1) Chen, D.; Tang, L.; Li, J. *Chem. Soc. Rev.* **2010**, *39*, 3157−3180.
(2) Geim, A. K. *Science* **2009**, *324*, 1530−1534.
(3) Dutta, S.; Pati, S. K. *J. Mater. Chem.* **2010**, *20*, 8207−8223.
(4) Novoselov, K.; Geim, A.; Morozov, S.; Jiang, D. *Science* **2004**, *306*, 666−669.
(5) Balandin, A. A.; Ghosh, S.; Bao, W.; Calizo, I.; Teweldebrhan, D.; Miao, F.; Lau, C. N. *Nano Lett.* **2008**, *8*, 902−907.
(6) Han, M.; Özyilmaz, B.; Zhang, Y.; Kim, P. *Phys. Rev. Lett.* **2007**, *98*, 206805.
(7) Zade, S.; Bendikov, M. *Angew. Chem., Int. Ed.* **2010**, *49*, 4012−4015.
(8) Konishi, A.; Hirao, Y.; Nakano, M.; Shimizu, A.; Botek, E.; Champagne, B.; Shiomi, D.; Sato, K.; Takui, T.; Matsumoto, K.; Kurata, H.; Kubo, T. *J. Am. Chem. Soc.* **2010**, *132*, 11021−11023.
(9) Fujita, M.; Wakabayashi, K.; Nakada, K.; Kusakabe, K. *J. Phys. Soc. Jpn.* **1996**, *65*, 1920−1923.
(10) Nakada, K.; Fujita, M.; Dresselhaus, G.; Dresselhaus, M. *Phys. Rev. B* **1996**, *54*, 17954−17961.
(11) Raghu, C.; Anusooya Pati, Y.; Ramasesha, S. *Phys. Rev. B* **2002**, *66*, 035116.
(12) Hikihara, T.; Hu, X.; Lin, H.-H.; Mou, C.-Y. *Phys. Rev. B* **2003**, *68*, 035432.
(13) Ezawa, M. *Phys. Rev. B* **2006**, *73*, 045432.
(14) Barone, V.; Hod, O.; Scuseria, G. E. *Nano Lett.* **2006**, *6*, 2748−2754.
(15) Al Hajj, M.; Alet, F.; Capponi, S.; Lepetit, M.; Malrieu, J.; Todo, S. *Eur. Phys. J. B* **2006**, *51*, 517.
(16) Sony, P.; Shukla, A. *Phys. Rev. B* **2007**, *75*, 155208.
(17) Gao, X.; Zhou, Z.; Zhao, Y.; Nagase, S.; Zhang, S. B.; Chen, Z. *J. Phys. Chem. C* **2008**, *112*, 12677−12682.
(18) Nakano, M.; Nagai, H.; Fukui, H.; Yoneda, K.; Kishi, R.; Takahashi, H.; Shimizu, A.; Kubo, T.; Kamada, K.; Ohta, K.; Champagne, B.; Botek, E. *Chem. Phys. Lett.* **2008**, *467*, 120−125.
(19) Wang, J.; Zubarev, D. Y.; Philpott, M. R.; Vukovic, S.; Lester, W. A.; Cui, T.; Kawazoe, Y. *Phys. Chem. Chem. Phy* **2010**, *12*, 9839.
(20) Son, Y.-W.; Cohen, M. L.; Louie, S. G. *Nature* **2006**, *444*, 347−349.
(21) Son, Y.-W.; Cohen, M. L.; Louie, S. G. *Phys. Rev. Lett.* **2006**, *97*, 216803.
(22) Hod, O.; Barone, V.; Peralta, J. E.; Scuseria, G. E. *Nano Lett.* **2007**, *7*, 2295−2299.
(23) Hod, O.; Barone, V.; Scuseria, G. *Phys. Rev. B* **2008**, *77*, 035411.
(24) Wang, W. L.; Meng, S.; Kaxiras, E. *Nano Lett.* **2008**, *8*, 241−245.
(25) Bhowmick, S.; Shenoy, V. *J. Chem. Phys.* **2008**, *128*, 244717.
(26) Philpott, M.; Cimpoesu, F.; Kawazoe, Y. *Mater. Trans.* **2008**, *49*, 2448.
(27) Qu, Z.; Zhang, D.; Liu, C.; Jiang, Y. *J. Phys. Chem. A* **2009**, *113*, 7909.
(28) Hajgato, B.; Huzak, M.; Deleuze, M. *J. Phys. Chem. A* **2011**, *115*, 9282.
(29) Wakabayashi, K.; Dutta, S. *Solid State Commun.* **2012**, *152*, 1420−1430.
(30) Dutta, S.; Wakabayashi, K. *Sci. Rep.* **2012**, *2*, 519.
(31) Houk, K. N.; Lee, P. S.; Nendel, M. *J. Org. Chem.* **2001**, *66*, 5517−5521.

(32) Bendikov, M.; Duong, H. M.; Starkey, K.; Houk, K. N.; Carter, E. A.; Wudl, F. *J. Am. Chem. Soc.* **2004**, *126*, 7416−7417.
(33) Hachmann, J.; Dorando, J. J.; Avilés, M.; Chan, G. K.-L. *J. Chem. Phys.* **2007**, *127*, 134309.
(34) Gidofalvi, G.; Mazziotti, D. *J. Chem. Phys.* **2008**, *129*, 134108.
(35) Jiang, D.-e.; Dai, S. *J. Phys. Chem. A* **2008**, *112*, 332−335.
(36) Pelzer, K.; Greenman, L.; Gidofalvi, G.; Mazziotti, D. *J. Phys. Chem. A* **2011**, *115*, 5632.
(37) Kobayashi, Y.; Fukui, K.-i.; Enoki, T.; Kusakabe, K.; Kaburagi, Y. *Phys. Rev. B* **2005**, *71*, 193406.
(38) White, S. R. *Phys. Rev. Lett.* **1992**, *69*, 2863−2866.
(39) White, S. R. *Phys. Rev. B* **1993**, *48*, 10345−10356.
(40) White, S. R.; Martin, R. L. *J. Chem. Phys.* **1999**, *110*, 4127−4130. Chan, G. K.-L.; Head-Gordon, M. *J. Chem. Phys.* **2002**, *116*, 4462−4476.
(41) Chan, G. K.-L.; Head-Gordon, M. *J. Chem. Phys.* **2002**, *116*, 4462−4476.
(42) Marti, K. H.; Ondk, I. M.; Moritz, G.; Reiher, M. *J. Chem. Phys.* **2008**, *128*, 014104.
(43) Kurashige, Y.; Yanai, T. *J. Chem. Phys.* **2009**, *130*, 234114.
(44) Pipek, J.; Mezey, P. *J. Chem. Phys.* **1989**, *90*, 4916−4926.
(45) Cuthill, E.; McKee, J.Reducing the bandwidth of sparse symmetric matrices. In *Proc. 24th Nat. Conf.*; ACM: New York, 1969; pp 157−172.
(46) Liu, W.; Sherman, A. *SIAM J. Numer. Anal.* **1976**, *13*, 198−213.
(47) Moritz, G.; Hess, B.; Reiher, M. *J. Chem. Phys.* **2005**, *122*, 024107.
(48) Del Corso, G.; Manzini, G. *Computing* **1999**, *62*, 189−203.
(49) Frisch, M. J. et al. *Gaussian 09*, revision A.1; Gaussian Inc.: Wallingford, CT, 2009.
(50) Neese, F. *ORCA*, version 2.8.0; University of Bonn: Bonn, Germany, 2010.
(51) Weigend, F.; Ahlrichs, R. *Phys. Chem. Chem. Phys.* **2005**, *7*, 3297−3305.
(52) Head-Gordon, M. *Chem. Phys. Lett.* **2003**, *372*, 508−511.
(53) Stück, D.; Baker, T.; Zimmerman, P.; Kurlancheek, W.; Head-Gordon, M. *J. Chem. Phys.* **2011**, *135*, 194306.
(54) Mizukami, W.; Kurashige, Y.; Yanai, T. *J. Chem. Phys.* **2010**, *133*, 091101.